Applied Physics A (2018) 124:211
https://doi.org/10.1007/s00339-018-1641-2

Applied Physics A
Materials Science & Processing

Phase-field simulation on dendritic to semi-circular morphology transition induced by forced liquid flow

Lifei Du[1] · Peng Zhang[1] · Shaomei Yang[1] · Zhongtang Gao[2] · Jie Chen[1] · Huiling Du[1]

Received: 4 November 2017 / Accepted: 1 February 2018 / Published online: 5 February 2018

Abstract
A 2-D phase-field model coupling with convection is implemented to investigate the dendritic morphology evolution of the Ni–40.8%Cu alloy during solidification with forced liquid flow. Simulation results indicate that liquid flow can significantly affect the distributions of temperature and concentration near the liquid–solid interface, leading to asymmetric formation of the dendritic microstructure. Increasing the liquid flow will enhance the asymmetry of dendrite morphology with much more suppressed growth in the downstream and intensified morphology development in the upstream, leading to a dendritic to semi-circular morphology transition in the microstructure formation. Based on the simulations, it can be concluded that the morphology changes with increasing flow velocity in this study is attributed to the difference of the constitutional supercooling near the solid–liquid interfaces, which is the result of the asymmetric solute diffusion induced by the liquid flow. Therefore, controlling the liquid flow during the solidification might lead to the microstructure optimization to achieve materials with excellent properties.

1 Introduction

Solidification is known as a very complex process accompanied with complex heat and mass diffusions. During metallic solidification, latent heat is released during the liquid to solid transition, leading to the interface moving continuously. In metallic alloys, the solute diffusion is significantly affected by temperature, pressure, liquid flow, and these factors would lead to changes of microstructures [1–5]. It has been widely established that the microstructures formed during the solidification process have great influences on properties of materials. Thus, in casting industries as well as metallic material researches, multi-scale microstructure controlling has become the most important way to improve the properties of materials. Recent studies have found that the convection can obviously affect the microstructure development during solidifications [6–10]. Liquid metal flow during solidifications can significantly affect the morphology, solute segregation at solid–liquid interfaces, and temperature distributions during solidification, by changing the heat and solute diffusions during the liquid–solid phase transition. However, the mechanism of solidification with convection is still unclear since it is too hard to observe in situ. Meanwhile, numerical simulation is an effective method for studying heat and solute diffusions during solidification, which are believed to be the main factors determining microstructure formations in metal alloys [11–17]. Thus, in this paper, the phase field method is implemented to investigate the dendritic growth of the Ni–Cu alloy with liquid flow, with the aim to study the effect of liquid flow on the microstructure formation during solidifications. Particularly, the heat and solute diffusions during solidification are analyzed to specify their relations on the morphology development with the liquid flow.

2 Phase field model and numerical method

In accordance with [18], this phase-field model for simulating the effect of liquid flow on the microstructure formation of a Ni–Cu alloy during solidification is employed. The main equations are listed below.

Phase field governing equation (in 2D) is

✉ Lifei Du
dulifei@xust.edu.cn

[1] College of Materials Science and Engineering, Xi'an University of Science and Technology, Xi'an 710054, China

[2] College of Mechanical Engineering, Xi'an University of Science and Technology, Xi'an 710054, China

$$\frac{\partial \phi}{\partial t} = M_\phi \bar{\varepsilon}^2 \left[\nabla \cdot \left(\eta^2 \nabla \phi \right) - \frac{\partial}{\partial x} \left(\eta \eta'_\beta \frac{\partial \phi}{\partial y} \right) + \frac{\partial}{\partial y} \left(\eta \eta'_\beta \frac{\partial \phi}{\partial x} \right) \right] - M_\phi \left[\left(1 - x_\mathrm{B} \right) H_\mathrm{A} + x_\mathrm{B} H_\mathrm{B} \right], \quad (1)$$

where M_ϕ is the interphase driving force-related phase field parameters, which is determined by $M_\phi = \left(1 - x_\mathrm{B}\right) M_\mathrm{A} + x_\mathrm{B} M_\mathrm{B}$ with $M_{\mathrm{A/B}} = \frac{\left(T_\mathrm{m}^{\mathrm{A/B}}\right)^2 \beta_{\mathrm{A/B}}}{6\sqrt{2}\left(\Delta H_{\mathrm{A/B}}\right)\lambda_{\mathrm{A/B}}} \cdot T_\mathrm{m}^\mathrm{A}$ and T_m^B are the melting point of pure A and pure B, respectively. ΔH_A and ΔH_B are the heat of fusion per volume. $\beta = \arctan\left((\partial\phi/\partial y) / (\partial\phi/\partial x) \right)$ gives an approximation of the angle between the interface normal and the orientation of the crystal lattice. $\bar{\varepsilon}$ is the parameter of the surface energy σ and the interface thickness λ; η is the parameter related to the interface anisotropy intensity, modulus and angle. H_A and H_B have the formula terms $H_{\mathrm{A/B}}(\phi, T) = W_{\mathrm{A/B}} g'(\phi) + 30 g(\phi) \Delta H_{\mathrm{A/B}} \left(\frac{1}{T} - \frac{1}{T_\mathrm{m}^{\mathrm{A/B}}} \right)$, where W_A and W_B are constants which can be calculated by $W_{\mathrm{A/B}} = \frac{3\sigma_{\mathrm{A/B}}}{\sqrt{2} T_\mathrm{m}^{\mathrm{A/B}} \lambda_{\mathrm{A/B}}}$. $g(\phi) = \phi^2 (1 - \phi)^2$ is a double-well potential with minima at $\phi = 0,\ 1$.

Solute conservation equation is

$$\frac{\partial x_\mathrm{B}}{\partial t} + \vec{V} \cdot \nabla x_\mathrm{B} = \nabla \cdot \left\{ D \left[\nabla x_\mathrm{B} + \frac{V_\mathrm{m}}{R} x_\mathrm{B} \left(1 - x_\mathrm{B}\right) \left(H_\mathrm{B}(\phi, T) - H_\mathrm{A}(\phi, T) \right) \nabla \phi \right] + \vec{j}_\mathrm{at} \right\}, \quad (2)$$

where x_B is the mole fraction of solute B in solvent A and $\vec{V}$ is the velocity vector. D is the diffusion coefficient and V_m is the mole volume. In binary alloys, $D = D_\mathrm{S} + p(\phi)\left(D_\mathrm{L} - D_\mathrm{S}\right)$, where D_L and D_S are the diffusion rates in the liquid and solid phases, respectively, and $p(\phi) = \phi^3 \left(10 - 15\phi + 6\phi^2\right)$ is a smoothing function. $\vec{j}_\mathrm{at}$ is the anti-trapping current to suppress the solute trapping due to the larger interface width used in simulations to get more quantitative predictions.

Temperature governing equation is

$$c_\mathrm{p} \left(\frac{\partial T}{\partial t} + \vec{V} \cdot \nabla T \right) + 30 g(\phi) \Delta \widetilde{H} \frac{\partial \phi}{\partial t} = \nabla \cdot K \nabla T. \quad (3)$$

In the formula, T is the temperature; C_p is the specific heat capacity; $\Delta \widetilde{H} = \left(1 - x_\mathrm{B}\right) \Delta H_\mathrm{A} + x_\mathrm{B} \Delta H_\mathrm{B}$; K is the thermal diffusion coefficient.

Continuity equation:

$$\nabla \cdot \left(\phi \vec{V} \right) = 0. \quad (4)$$

Momentum equation:

$$\frac{\partial \phi \vec{V}}{\partial t} + \phi \left(\vec{V} \cdot \nabla \right) \vec{V} = -\frac{\phi}{\rho} \nabla P + \nu \nabla^2 \left(\phi \vec{V} \right) - \frac{\nu h (1 - \phi^2) \phi \vec{V}}{\lambda^2}, \quad (5)$$

where P, ρ, and $\nu$are the liquid flow velocity, pressure, density, and kinematic viscosity, respectively. $\vec{M}_\mathrm{d}$ is the dissipative interfacial stress. A detail description for this phase-field model with convection can be found in Ref [18].

In the present work, a seed with an initial radius is assumed to nucleate in the domain at the beginning. The zero-Neumann boundary conditions are used in the calculation of phase field, solute field and temperature field. Equations (1–3) are discretized using a finite difference approach with a uniform spatial lattice. The total number of grids is $1200\Delta x \times 1200\Delta y$ with $\Delta x = \Delta y = 1.0 \times 10^{-8}$ m, and the corresponding time step $\Delta t = 5.0 \times 10^{-8}$ s. A circular solid seed is set at (600, 400) with a radius of $6\Delta x$. The continuity Eq. (4) and Navier–Stokes Eq. (5) were solved with the semi-implicit method for pressure-linked equation (SIMPLE) scheme under zero-Neumann boundary conditions for left and right boundaries, and the initial flow direction is set to be from top to the bottom of simulation zone, with top boundary as the flow input boundary and the bottom boundary is set to be the flow output boundary. Based on the physical parameters of the Ni–Cu alloy, which can be calculated from parameters of pure Cu and Ni (as shown in Table 1) based on the simple linear mixing method, the Prandtl number of the melt is about 0.002 and the Schmidt number is about 6.0. This indicates the flow would not have significant influence on the temperature distribution, but the solute diffusion would be significantly changed by the liquid flow. Thus, with zero-Neumann boundary conditions, the effect of the initial liquid flow on the morphology evolution can be investigated with this simulation domain since the solute diffusion can also determine the phase transition

Table 1 Physical parameters used in the simulations

Parameter	Value
T_M^A—melt temperature of Ni (K)	1728.0
T_M^B—melt temperature of Cu (K)	1358.0
ΔH_A—latent heat of Ni (J/m^3)	2.35×10^9
ΔH_B—latent heat of Cu (J/m^3)	1.728×10^9
K_A—heat conductivity of Ni (W/mK)	84.0
K_B—heat conductivity of Cu (W/mK)	200.0
c_A—specific heat of Ni (J/m^{3}K)	5.42×10^6
c_B—specific heat of Cu (J/m^{3}K)	3.96×10^6
D_L—diffusion coefficient of the liquid phase (m^2/s)	1.0×10^{-9}
D_S—diffusion coefficient of the solid phase (m^2/s)	1.0×10^{-13}
V_m—mole volume of alloy (m^3/mol)	7.42×10^{-6}
σ_A—surface energy of Ni (J/m^2)	0.37
σ_B—surface energy of Cu (J/m^2)	0.29
β_A—interface kinetic coefficient of Ni (m/sK)	3.3×10^{-3}
β_B—interface kinetic coefficient of Cu (m/sK)	3.9×10^{-3}
λ—interface thickness (m)	4.9×10^{-8}
γ—magnitude of anisotropy	0.04

during solidifications by changing the solute segregation near solid–liquid interfaces.

3 Results and discussion

From the discussion in the previous studies [17–23], we can conclude that the liquid flow in the presence of solidifying interfaces can significantly change the morphology evolution by altering the solute and heat diffusions near solid–liquid interfaces, and the asymmetric development of dendrites is believed to be enhanced with the increasing intensity of the liquid flow. The morphology transition with increasing liquid flow is to be simulated, and the interface morphology is plotted in Fig. 1.

Without liquid flow, the solidifying morphology is the typical dendrite with weak side branches, and all side branches are oriented in the direction of primary dendrite arms due to the kinetic anisotropy. With relatively small initial liquid flow, the dendritic growth shows an asymmetric developing: in the upstream, the dendrite developing is enhanced and the secondary arms are all oriented in the direction of the initial flow field, while in the downstream primary dendrite arm and all secondary arms are suppressed. With increasing liquid flow intensity, asymmetric solidifying in upstream and downstream is significantly enhanced, and side branches in both downstream and upstream change in two different ways: side branches in the downstream intend to vanish while side branches in the upstream are combined into a continuous solid phase due to the different solidifying rate caused by the liquid flow. It is particularly important to note that though no side branches can be found when the initial liquid flow is larger than 0.15 m/s, the secondary dendrite arms in the upstream can be considered to combine into a continuous solid phase, while in the downstream the secondary dendrite arms are continuously suppressed till disappearing. With further increase of the initial liquid flow, the solidifying morphology begins to take on new characteristics: anisotropy of the solid phase growing is qualitatively changed, and growth superiority of the primary dendrite arms is unapparent with increasing liquid flow. A semi-circular solid is formed in the downstream region with a liquid flow of 0.3 m/s. There is an obvious dendrite to semi-circular morphology transition with increasing liquid flow. To characterize the effect of liquid flow on microstructure evolution, the distance of solid–liquid interface positions from the initial dendrite center is measured and plotted in Fig. 1b. Representative positions are selected from the intersections of the solid–liquid interface and curves of different included angle with respect to the rectangular coordinate axes, as labeled in Fig. 1a. It is obvious that the growth rate of the dendrite tip in the upstream is significantly higher than those of other regions. With increasing initial flow field, the growth rate difference of each region is gradually reduced, indicating that when the flow field is greater than a certain value, the dendrite intends to a spherical shape in the upstream region.

Figure 2 shows the concentration distribution maps at 2.0 ms for dendritic growth under different forced liquid flow, and the corresponding temperature distribution maps are plotted in Fig. 3. With induced liquid flow, the solute diffusion is changed asymmetrically in the whole region,

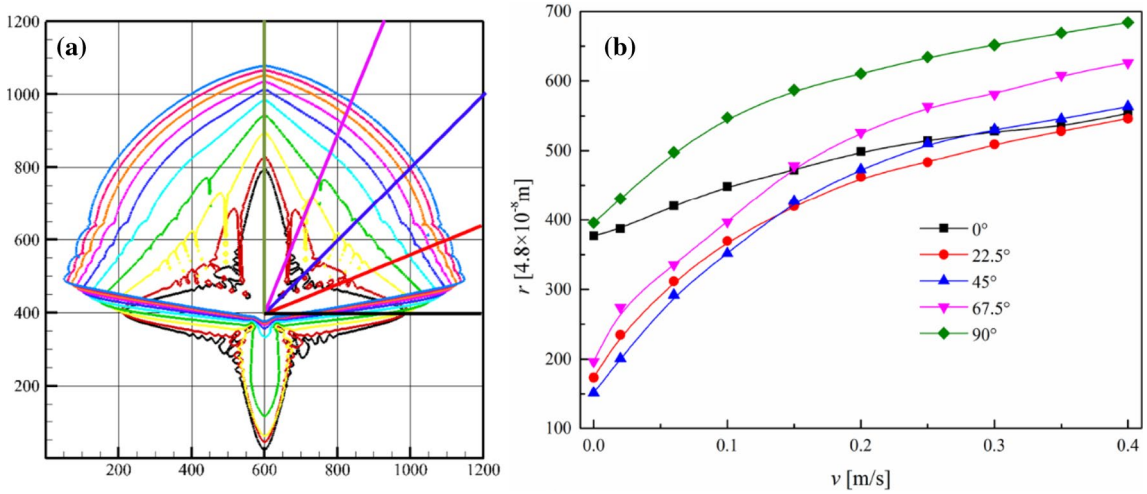

Fig. 1 Dendritic morphology during dendritic growth process under liquid flow (0 ~ 0.4 m/s) at the same time step. **a** Solid–liquid interface morphology. The color loop curves from inner to outer represent solid–liquid interfaces with initial velocities of 0, 0.02, 0.06, 0.10, 0.15, 0.20, 0.25, 0.30, 0.35 and 0.40 m/s. **b** Interface distances from the initial dendrite center detected along the colored straight lines in **a**, which have different included angles: 0.0°, 22.5°, 45.0°, 67.5°, 90.0°

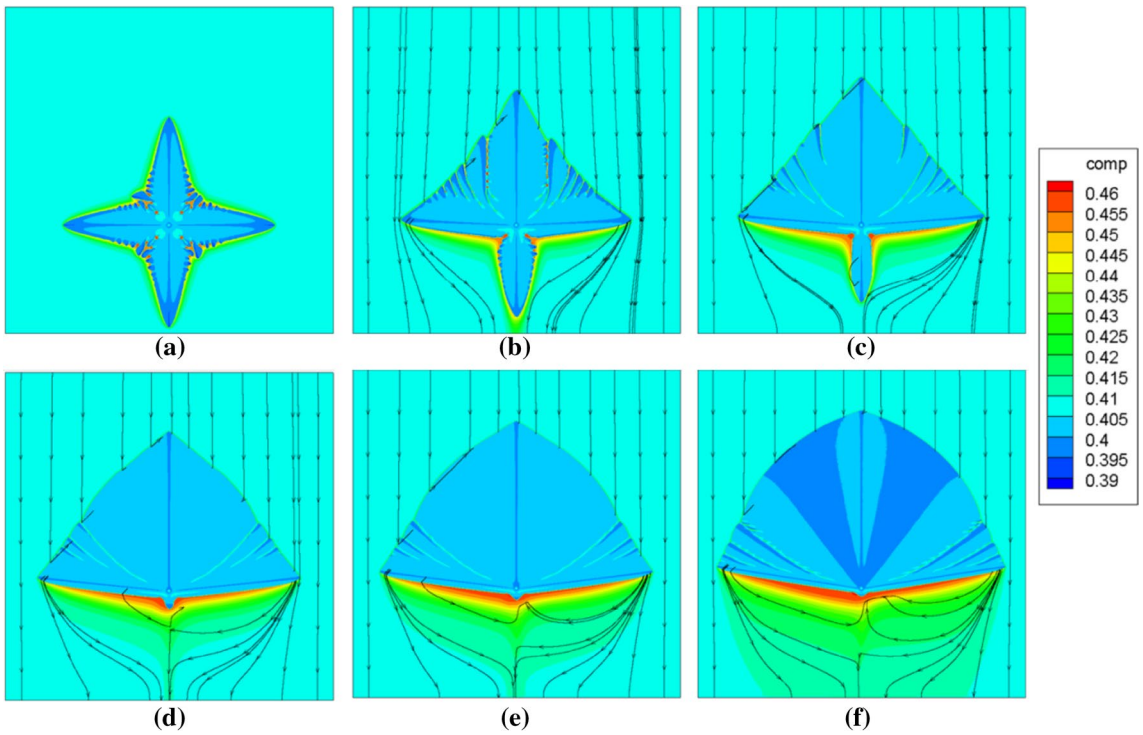

Fig. 2 Concentration distribution in dendritic growth process at $t=2.0$ ms. **a** $v=0$ m/s; **b** $v=0.05$ m/s; **c** $v=0.10$ m/s; **d** $v=0.15$ m/s; **e** $v=0.20$ m/s; **f** $v=0.30$ m/s

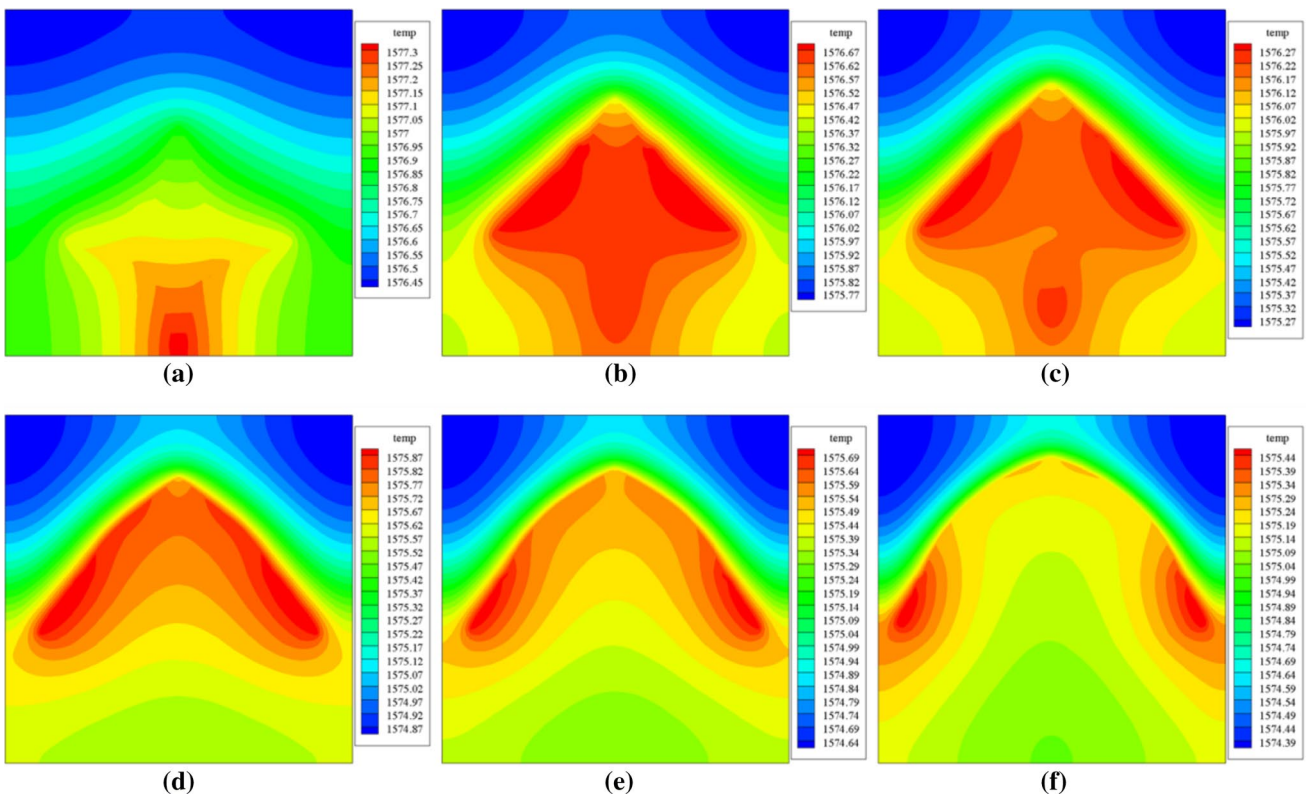

Fig. 3 Temperature distribution in dendritic growth process at $t=2.0$ ms. **a** $v=0$ m/s; **b** $v=0.05$ m/s; **c** $v=0.10$ m/s; **d** $v=0.15$ m/s; **e** $v=0.20$ m/s; **f** $v=0.30$ m/s

leading to solute segregation discrepancy at interfaces in different regions. Liquid flow moves the solute from the upstream of the flow field to the downstream, and the vortex, as the result of interaction between growing dendrite and initial liquid flow, leads to solute enrichment so that enhanced solute segregation is formed at the interface in the downstream. This large difference of the solute distribution around the dendrite could be the reason for the asymmetrical morphology formation with induced liquid flow. The temperature distributions are mostly determined by the lantern heat since the high temperature is located at solid–liquid interfaces, since the influence of liquid flow on the temperature distribution could be negligible within the limited time frame with Prandtl number $P_r = 0.002$ in this study.

To further specify reason for the microstructure transition induced by the liquid flow, the concentration and temperature distribution profiles on the primary dendrite arm in the vertical direction ($X = 600\Delta x$, from the bottom to the top) with different initial liquid flow are plotted in Fig. 4. It is obvious that the solute partitions in the downstream regions are much higher than that in the upstream, while temperature in the upstream is higher than that in the downstream region as the result of large latent heat release from the liquid–solid phase transition. It has been well established that during solidification in metal alloys, the constitutional supercooling at the solid–liquid interface caused by the solute partition is the main factor determining the phase transitions. With increasing initial liquid flow, the solute partition difference induced by the liquid flow intends to be enlarged. Considering the dendrite morphology shown in Fig. 1, we can clearly conclude that with large initial liquid flow, the main reason resulting in the dendritic to semi-circular morphology transition in this study is the large solute distribution difference caused by the liquid flow, which has already been discussed in detail in previous studies on liquid flow on solidifications [16, 18].

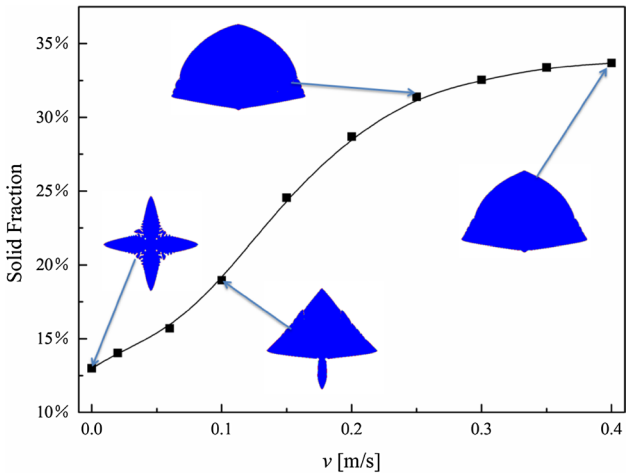

Fig. 5 Solid rate change with increasing initial liquid flow

In Fig. 5, the solid fraction of the simulation zone at the same time step ($t = 2.0$ ms) is measured and plotted as a function of initial liquid flow. With increasing initial liquid flow, the solid phase shows a non-linear increasing characteristic: rapidly increasing with increasing liquid flow and the increasing rate decreases with large liquid flow. In our simulations, the only heat input into the simulation zone is the latent heat release from the liquid–solid phase transition, thus with increasing solid phase rate, the temperature should be higher. However, as shown in Fig. 4b, the temperature with large initial liquid flow is lower along the primary dendrite arm. Comparing with the temperature distributions in Fig. 3, dendrite formation is enhanced in the upstream with higher temperature, which could further confirm that the morphology transition investigated in this study is attributed to the asymmetrical solute diffusion induced by the liquid flow.

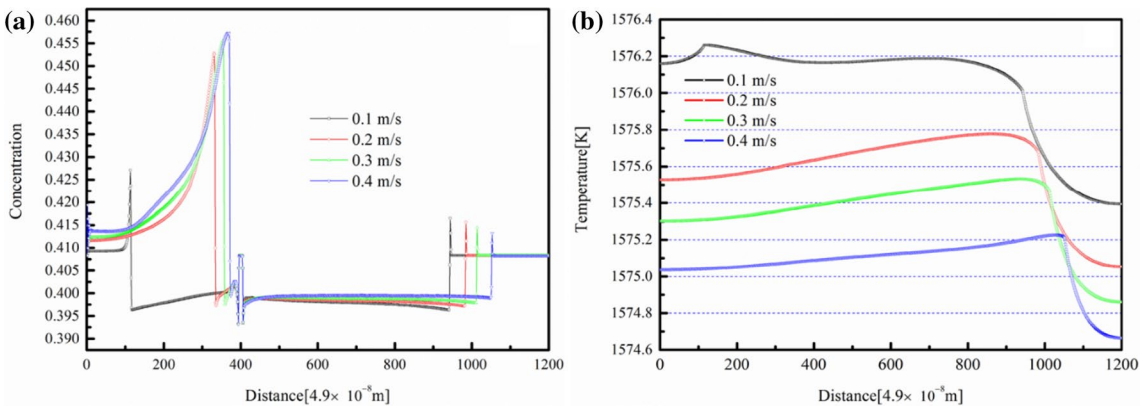

Fig. 4 Concentration (**a**) and temperature (**b**) distribution profiles of primary dendrite arm with different initial liquid forced flow

4 Concluding remarks

Liquid flow has a significant effect on the dendrite microstructure formation by changing the solute and heat diffusions during the solidification. In this paper, the dendritic growth and microstructure development with initial liquid flow were simulated by the 2-D phase field method to investigate the microstructure formation with initial liquid flow. The effect of liquid flow on heat transfer is neglected due to the limited size of simulation zone and parameters used in this study. The liquid flow during solidification can largely influence the solute diffusion during solidification, leading to solute segregation difference at solid–liquid interfaces in the downstream and upstream, which would result in the irregular dendrite development. A dendritic to semi-circular morphology transition can be observed with increasing initial liquid flow. By analyzing the concentration and temperature distributions in the simulation zone, the dendrite to semi-circular transition is believed to be attributed to the constitutional supercooling differences in the upstream and downstream sides induced by the liquid flow.

Acknowledgements This work was supported by the National Natural Science Foundation of China (Grant numbers 51501146, 21503165, 51701152, 51602252, 51705415, 51372197), the Cultivating Research Program of Xi'an University of Science and Technology (Grant number 201701), and the Key Innovation Team of Shaanxi Province (Grant number 2014KCT-04).

References

1. M. Asta, C. Beckermann, A. Karma, W. Kurz, R. Napolitano, M. Plapp et al., Solidification microstructures and solid-state parallels: recent developments, future directions. Acta Mater. **57**, 941–71 (2009)
2. W.J. Boettinger, S.R. Coriell, A.L. Greer, A. Karma, W. Kurz, M. Rappaz et al., Solidification microstructures: recent developments, future directions. Acta Mater. **48**, 43–70 (2000)
3. M.E. Glicksman, Principles of solidification. Mater. Today **14**, 502 (2011)
4. W. Kurz, D.J. Fisher, *Fundamentals of Solidification*, 4th edn. (Trans Tech Publications Ltd, Zurich, 1998), pp. 71–92
5. Y. Ali, D. Qiu, B. Jiang, F. Pan, M.X. Zhang, Current research progress in grain refinement of cast magnesium alloys: a review article. J. Alloys Comp. **619**, 639–51 (2015)
6. X. Li, D. Du, A. Gagnoud, Z. Ren, Y. Fautrelle, R. Moreau, Effect of multi-scale thermoelectric magnetic convection on solidification microstructure in directionally solidified Al–Si alloys under a transverse magnetic field. Metall. Mater. Trans. A **45**, 5584–600 (2014)
7. C.Y. Wang, C. Beckermann, Equiaxed dendritic solidification with convection: part I. Multiscale/multiphase modeling. Metall. Mater. Trans. A **27**, 2754–2764 (1996)
8. L. Wang, J. Shen, S. Zhao, L. Wang, F.U. Hengzhi, Phase and microstructure selection in directionally solidified peritectic alloys under convection condition. Acta Metall. Sin. **49**, 822 (2013)
9. L. Yuan, P.D. Lee, Dendritic solidification under natural and forced convection in binary alloys: 2D versus 3D simulation. Model. Simul. Mater. Sci. Eng. **18**, 055008 (2010)
10. Y. Chen, H. Nguyenthi, D.Z. Li, A.A. Bogno, B. Billia, N.M. Xiao, Influence of natural convection on microstructure evolution during the initial solidification transient: comparison of phase-field modeling with in situ synchrotron X-ray monitoring data. IOP Conf. Ser. **33**, 012102 (2012)
11. N. Al-Rawahi, G. Tryggvason, Numerical simulation of dendritic solidification with convection: three-dimensional flow. J. Comput. Phys. **194**, 677–96 (2004)
12. D. Samanta, N. Zabaras, Modelling convection in solidification processes using stabilized finite element techniques. Int. J. Numer. Meth. Eng. **64**, 1769–1799 (2010)
13. T.V. Vu, Three-phase numerical simulations of solidification with natural convection in a vertical cylindrical annulus. Int. J. Multiph. Flow. **95**, 120–134 (2017)
14. M. Wu, A. Fjeld, A. Ludwig, Modelling mixed columnar-equiaxed solidification with melt convection and grain sedimentation—part I: model description. Comput. Mater. Sci. **50**, 32–42 (2011)
15. M. Zhu, D. Sun, S. Pan, Q. Zhang, D. Raabe, Modelling of dendritic growth during alloy solidification under natural convection. Model. Simul. Mater. Sci. Eng. **22**, 034006 (2014)
16. L.F. Du, R. Zhang, L.M. Zhang, Phase-field simulation of dendritic growth in a forced liquid metal flow coupling with boundary heat flux. Sci. China Technol. Sci. **56**, 2586–2593 (2013)
17. L. Qiang, Y. Xiangjie, L. Zhiling, Influence of the melt flow rate on dendrite micro segregation during alloy solidification simulated by phase field method. J. Appl. Sci. **13**, 2700–2704 (2013)
18. L. Du, R. Zhang, Phase-field simulation of concentration and temperature distribution during dendritic growth in a forced liquid metal flow. Metal. Mater. Trans. B **45**, 2504–2515 (2014)
19. Z. Guo, J. Mi, S. Xiong, P.S. Grant, Phase field simulation of binary alloy dendrite growth under thermal- and forced-flow fields: an implementation of the parallel–multigrid approach. Metal. Mater. Trans. B **44**, 924–37 (2013)
20. C.W. Lan, C.J. Shih, Phase field simulation of non-isothermal free dendritic growth of a binary alloy in a forced flow. J. Cryst. Growth. **264**, 472–82 (2004)
21. W.Y. Long, D.L. Lü, C. Xia, M.M. Pan, Q.Z. Cai, L.L. Chen, Phase-field simulation of non-isothermal solidification dendrite growth of binary alloy under the force flow. Acta Phys. Sin. **58**, 7802–7808 (2009)
22. R. Siquieri, J. Rezende, J. Kundin, H. Emmerich, Phase-field simulation of a Fe–Mn alloy under forced flow conditions. Eur. Phys. J. Spec. Top. **177**, 193–205 (2009)
23. X. Yuan, Y. Yang, Phase field simulation of dendrite growth of Fe–C alloy in a forced flow. *MMAT-12*. 2013, pp. 602–604